Rayleigh scattering from crystals and amorphous structures

O. D. Gonçalves and W. M. S. Santos
Instituto de Física da Universidade Federal do Rio de Janeiro, Caixa Postal 68528, Rio de Janeiro, Codigo de Enderecamento Postal 21941, Rio de Janeiro, Brazil

J. Eichler
Technische Fachhochschule Berlin, 1000 Berlin 65, Germany

A. M. Borges
Instituto de Física da Universidade Federal Fluminense, Caixa Postal 100296, Niteroi, Codigo de Enderecamento Postal 24020, Rio de Janeiro, Brazil

(Received 22 September 1992)

Elastic-scattering cross sections of photons for momentum transfer in the range $0.1 \leq x \leq 2.2$ Å^{-1} with $E_\gamma = 59.5$ and 316 keV were measured in order to test the limits of momentum transfer within which the scattering by real samples can be considered as being due to free-atom Rayleigh scattering. Polycrystalline aggregate, liquid, perfect-single-crystal, and crystal powder samples were used as scatterers. The measurements for $E_\gamma = 316$ and 59.5 keV were carried out in the angular ranges $\theta = 0.5°-10°$ and $2°-23°$ with a geometrical resolution of 0.1° and 1°, respectively. At the present time, most of the experimental data on elastic photon scattering have been measured using solid molecular structures as scatterers. The present results allow the conclusion that highly precise data ($\Delta d\sigma/d\Omega \leq 2\%$) on elastic scattering of photons can be compared with free-atom Rayleigh-scattering theories only for $x > 2$ Å^{-1}.

PACS number(s): 32.80.Cy, 32.90.+a

INTRODUCTION

Elastic scattering of photons is an important process to obtain information about atomic wave functions and structures, to test perturbational theories and associated computational methods. These data are important in many interdisciplinary problems where the information about the interaction between photons and matter plays a very important role. From the solid-state point of view, an accurate knowledge of the interaction between photons and free atoms is required for understanding interference effects due to molecular structures.

In the low-energy range, under 100 keV and near the absorption edges, the elastic-scattering process (known as *anomalous scattering*) is particularly important due to the strong variation of the scattering cross section with the incident photon energy. Many experiments were performed in order to measure the elastic cross section and many of them were compared with Rayleigh-scattering theories [1], where it is assumed that the atoms are free.

In a former work [2,3] we have reported the occurrence of interference effects in photon scattering by polycrystalline aggregates due to Bragg scattering. It was shown that for low-momentum transfer, the scattering cannot be explained as being due to free atoms being necessary to consider solid-state scattering processes. On the other hand, for high-momentum transfer, due to the thermal vibration of the atoms, the free-atom model is a good approximation. The limit for the application of the free-atom model was found to be ($x \geq 2$ Å^{-1}), where x is related to momentum transfer and is described as

$$x = \lambda^{-1} \sin(\theta/2) ,$$

where $\lambda^{-1} = E/12.398$, E is the energy of the incident photon in keV, and θ is the scattering angle.

In this work, we study elastic scattering by liquid (Hg), perfect crystal (Si), and powder (Si) samples in order to verify the occurrence of interference effects in molecular structures other than polycrystals. We have also studied the limit between the scattering regimes with 145-keV photons and a high-resolution experimental setup to test if the momentum transfer is a good scaling for the scattering intensities in this range of x.

THEORY

Elastic-scattering amplitudes of photons by atoms, with photon energy ranging from a few keV to MeV, are usually calculated with the assumption that the atoms are free [free-atom approximation (FAA)]. The most common of such calculations are based on the form-factor approximation (FFA) either in the nonrelativistic, relativistic, or in the modified relativistic version. Extensive tables were published by Schaupp *et al.* [4] and Hubbel *et al.* [5]. In this approximation, the scattering intensity due to a free electron is multiplied by the Fourier transform of the electronic density. Different ways of obtaining the electron wave functions correspond to different form factors. The best agreement with experimental data was obtained with the modified relativistic form factor (MRFF) also called the G factor. The wave functions are in this case obtained from a Dirac-Hartree-Fock calculation considering spherical symmetry for the atom.

The most complete (and computer time-consuming) approach is the second-order perturbation theory, first developed by Brown, Peierls, and Woodward [6] and im-

proved by Kissel, Pratt, and co-workers [7,8]. The method is still a one-particle model, but considers all possible (permitted and forbidden) transitions to intermediate states in the scattering process.

Both methods are described in detail in Ref. [7]. A comparison between different theories and experimental data for $x > 1$ can be found in Refs. [8] and [9].

For $x < 2$ Å^{-1}, the cooperative effects due to the aggregate state of the atoms in the sample may render meaningless the direct comparison of the experimental data on the Rayleigh cross section with the results of free-atom theories. In considering the transition between both scattering regimes (by free atoms and correlated atoms) it is possible, although not completely true, to suppose that the elastic scattering of photons by atomic electrons is well described by the form-factor approximation.

Following Azároff [10], for low-momentum transfer (where the form-factor approximation is expected to be valid), the intensity of elastic-scattered radiation (energy by unit area by unit time at a distance R from the scatterer) from many atoms samples, is given in electron units by

$$I_s = I_e f^2 \sum_m \sum_n e^{i\mathbf{K}\cdot(\mathbf{R}_m - \mathbf{R}_n)} ,$$
$$I_e = r_0^2 / R^2 [(1+\cos^2\theta)/2] , \tag{1}$$

where I_e is the Thomson scattering intensity at a distance R from the electron, I_0 is the intensity of incident radiation, r_0 is the classical electron radius, θ is the scattering angle, f_m, f_n are the atomic form factors, $\mathbf{R}_m$ ($\mathbf{R}_n$) is the position of the mth (nth) atom, and $|\mathbf{K}| = 4\pi x / h$ is the momentum transfer.

In solving Eq. (1) we should consider how the atoms are placed in the sample. For a single crystal, in which the atoms could have just small displacements around the original positions in a cell, we have shown [3] that the term $\mathbf{K}\cdot(\mathbf{R}_m - \mathbf{R}_n)$ could be taken as

$$e^{i\mathbf{K}\cdot(\mathbf{R}_m - \mathbf{R}_n)} e^{i\mathbf{k}\cdot(\mu_m - \mu_n)} ,$$

where μ_m (μ_n) are the instant atomic displacement of the mth (nth) atom from the original position in the crystal cell. The scattering intensity can then be written as

$$I_s = I_e f^2 N(1 - e^{-2M}) + I_{\text{Bragg}} e^{-2M} , \tag{2}$$

where I_{Bragg} is the Bragg scattered intensity without considering thermal vibrations and e^{-2M} is the Debye factor, proportional to the momentum transfer and to the temperature.

Similar to the polycrystal case [3], we expect that for perfect crystals and crystal powder samples the application of the free-atom approximation will depend on the sample (chemical element and atomic structure) and on experimental parameters (momentum transfer, geometrical resolution of the setup, and temperature). The only difference is that for a perfect crystal, the detection of the diffraction peaks depends on the orientation of the sample. By choosing the sample orientation in the experimental setup, it is possible to avoid the Bragg peaks. In this case the scattered detected photons are due to thermal diffuse scattering, and the free-atom approximation is applicable.

For liquids the process is quite different. In this case there is a short-range order, but it is much larger than in a crystal. The atoms are not linked to a fixed position, but can move in any direction inside a small volume. In this case, the summation over m and n in Eq. (1) could be changed [10] by an integral over the possible values of $\mathbf{r}_{mn} = \mathbf{R}_m - \mathbf{R}_n$:

$$I_s = I_e f^2 N \left[1 + \int 4\pi r^2 \rho(r) \frac{\sin(kr_{mn})}{kr_{mn}} dr \right] . \tag{3}$$

Following this and different from the crystal case, the oscillations in the scattered photon intensity are expected to be broad, independent of the experimental angular resolution. For high-momentum transfers the function $\sin(kr)/kr$ tends to zero, making the free-atom model applicable. The next item will present experimental data obtained in order to investigate the limits for which the free-atom scattering models apply.

EXPERIMENTAL PROCEDURE

Two experiments were performed depending on the photon energy used. The first experiment was performed at the Nuclear Physics Department of the Universidade Federal do Rio de Janeiro. The relative elastic-scattering differential cross section $(d\sigma/d\Omega)_{\text{rel}}$ was measured for polycrystalline aggregate (Pb and Si), for a perfect crystal (Si), and for a liquid sample (Hg). The experimental setup was the same as that described in Ref. [2] using an americium γ-ray source (Am^{241}, $E_\gamma = 59.5$ keV, $I = 100$ mCi). The polycrystalline samples used were lead (0.137 g/cm^2) and silicon crystal powder (1.196 g/cm^2). The perfect crystal was Si (3.215 g/cm^2). Mercury (0.487 g/cm^2), inside a Plexiglas capsule 0.25 mm thick, was used as the liquid sample.

The second experiment was performed at the Hahn-Meitner Institut of Berlin, with a strong iridium γ-ray source (^{192}Ir, $E_\gamma = 316$ keV, $I = 50$ Ci). The experimental setup was similar to that used at 59.5 keV, but with much higher geometric accuracy (0.1° described elsewhere [11]). The targets used were a polycrystalline aggregate (Pb, 3.40 g / cm^2), a perfect crystal (Si, 4.66 g/cm^2), and a liquid sample, which consisted of 2.70 g/cm^2 of Hg, in a glass capsule 1.0 mm thick. The results for the liquid samples were corrected by subtracting the contributions for the scattered photon intensity due to the capsule material which was measured separately.

RESULTS

The experimental results are presented in Figs. 1–3. The results are compared with theoretical calculations which include Compton- and Rayleigh-scattering cross sections. The Compton cross sections were obtained from the incoherent-scattering functions [5], while the theoretical Rayleigh cross sections were obtained from the modified-form-factor approximation [4], or performed by Kissel [12] using the second-order pertubation

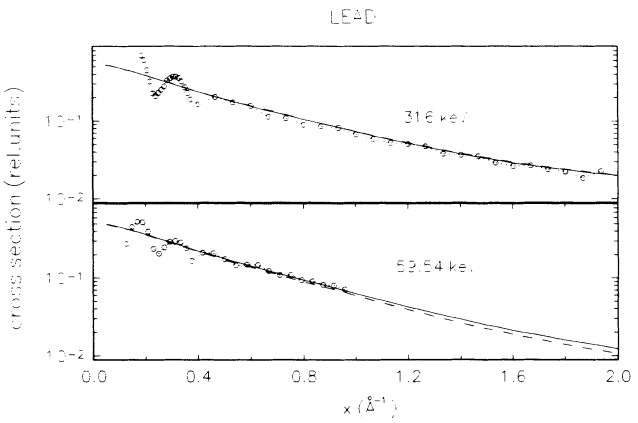

FIG. 1. Comparison between experimental scattering cross sections (circles) for Pb with 59.54- and 316-keV γ-ray and free-atom scattering theories. Theoretical curves were obtained from the form-factor approximation [4] (solid lines) and second-order pertubation theory [7] (dashed lines) added to the Compton cross sections obtained with the incoherent-scattering factor [5]. The dotted lines binding experimental points are only a guide to the eye. Experimental errors ($\leq 7\%$) are smaller than the point size.

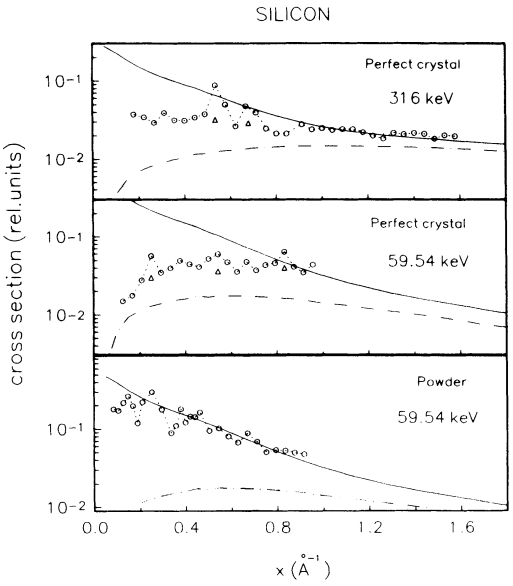

FIG. 3. Same as Fig. 1 for the Si perfect crystal (59.54 and 316 keV) and Si powder (59.54 keV). The smooth dot-dashed lines are the Compton (inelastic) scattering cross sections plotted to compare with the total scattering cross sections.

theory as developed by Kissel, Pratt and co-workers [7,8]. It is a numerical method within the framework of external field quantum electrodynamics and a description of independent bound atomic electron states in a relativistic self-consistent central potential. Due to limitations in computer time, outer subshell amplitudes are obtained with modified-form-factor approximation. Although many cases were already published [8], a complete tabulation is still not available.

Since we are interested in a relative differential cross section, this was obtained from

$$\frac{d\sigma}{d\Omega_{\rm rel}} = N(Z,E,\Omega,\theta)\frac{1}{F_{\rm att}(Z,\theta_i,\theta_s)} ,$$

where $N(Z,E,\Omega,\theta)$ is the count rate of the scattered radiation. $1/F_{\rm att}(Z,\theta_i,\theta_s)$ is the correction for γ attenuation for both incident and scattered beam. For normal incidence ($\theta_i = 90°$) and $\theta = \theta_s$, $1/F_{\rm att}$ is given by

$$\frac{1}{F_{\rm att}} = -\frac{e^{-\mu a} - e^{-\mu a/\cos\theta_s}}{a\mu(1-1/\cos\theta_s)} ,$$

where a is the sample thickness in g/cm^2, and μ is the total attenuation coefficient in cm^2/g. The error associated with the experimental momentum transfer is given by

$$\delta x = A\{[(E/2)\cos(\theta/2)\delta\theta]^2 + [\sin(\theta/2)\delta E]^2\}^{1/2} ,$$

where E is the photon energy, θ is the scattering angle, and $A = 1/12.398$ (Å^{-1} keV^{-1}).

For both photon energies (316 and 59.54 keV) the resulting momentum-transfer accuracies have the same order of magnitude (0.1 and 0.2 Å^{-1}), which makes it possible for a direct comparison between both experimental data. In order to compare measured and theoretical data, and since the obtained experimental data are relative cross sections, it was necessary to multiply the theoretical values by a normalization factor obtained from

$$C = \left[\frac{d\sigma(\alpha)}{d\Omega}\right]_{\rm expt}\left[\left[\frac{d\sigma(\alpha)}{d\Omega}\right]_{\rm Rayleigh} + \left[\frac{d\sigma(\alpha)}{d\Omega}\right]_{\rm Compton}\right]^{-1}_{\rm theoretical} ,$$

where α is a chosen scattering angle in a region where no interference effects were expected.

In the considered range of momentum transfer (0.05 and 2.0 Å^{-1}), the maximum Compton shift is 1.0 keV for

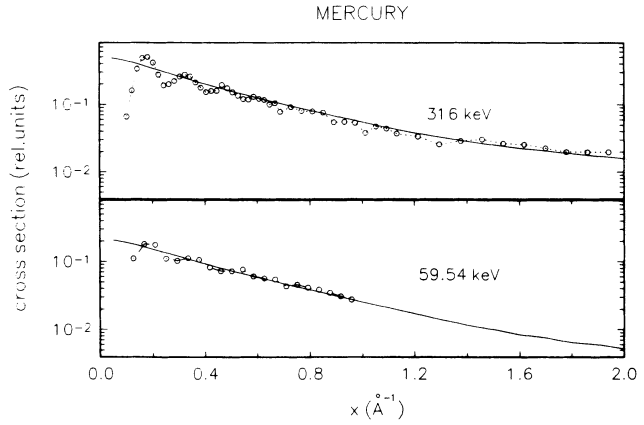

FIG. 2. Same as Fig. 1 for Hg. It was not included in the second-order pertubation theory curve. The dotted-line binding experimental points are only a guide to the eye. Experimental errors ($\leq 7\%$) are smaller than the point size.

59.5 keV and 3.0 keV for 316 keV, which does not allow us to distinguish the elastic from the inelastic process. For Pb and Hg the maximum contribution from Compton to scattered amplitude is 7%, while for silicon it rises up to 70%. The peculiarities of each measurement with different structures are described in the next items.

A. Polycrystalline aggregate and crystal powder

Metal structures and crystal powder are similar in describing the scattering process [3]. As reported early for metals, the observed oscillations are due to interference effects (Bragg peaks) convoluted with the geometrical accuracy of the experimental setup [2].

The measurement with lead, already reported [2], was repeated in order to control the experimental conditions and also to compare the results with the new 316-keV data. The results for Pb and Si are presented in Figs. 1 and 3. In Fig. 1 it is possible to notice that, for lead and $x \geq 0.5$ Å^{-1}, the experimental data show a good agreement with both calculations. Also, for silicon powder (Fig. 3), it is possible to notice that, depending on the desired accuracy, the free-atom model could be used to describe the experimental data for $x \geq 0.5$ Å^{-1}.

B. Perfect crystals

The experiment performed with the perfect single crystal of Si was done trying to avoid the Bragg conditions. This was done by fixing the incidence angle in 90°. In this case, the interference between the elastic-scattered photons is expected to be destructive, and no elastic-scattered photon should be detected.

Owing to the angular divergence of the beam, the Bragg diffraction could not always be avoided, resulting in diffraction peaks for $x = 0.53$ and 0.67 Å^{-1} for 316 keV and peaks for $x = 0.26$, 0.53 and 0.83 Å^{-1} for 59.5 keV (Fig. 3). For the corresponding scattering angles, a new data set was measured by rotating the crystal in order to avoid the Bragg conditions. As expected, the scattered intensities were drastically reduced (points marked as Δ in Fig. 3).

From the experimental results for Si it is possible to say that the free-atom approximation applies for $x \geq 1.0$ Å^{-1}. The remaining scattered photon intensity is due to Compton scattering and to thermal diffuse scattering (TDS) and this procedure can be used as a new way to measure these two effects.

C. Amorphous structure (liquid)

Figure 2 shows the results for mercury (59.54 and 316 keV). As described in Ref. [13], the interference effect in this case is due to a molecular correlation which represents a mean distance between the molecules. It implies that the obtained interference peaks depend weakly on the geometrical resolution. As in the metals, the more the momentum transfer grows the more the thermal motion of the molecules will grow, which makes the free-atom model applicable for high-momentum transfer. In Fig. 2, it is possible to observe that the x limit for the application of the free-atom model for mercury lies around 0.6 Å^{-1}.

CONCLUSIONS

The agreement between both data sets on both energies is very good, confirming that momentum transfer is a good choice to scale the dependence of the scattered photon intensity with angle and energy in low-momentum-transfer range. From the two experimental data sets it is possible to conclude that, for each atomic structure, there are limits above which the free-atom approximation applies. These limits depend on the temperature, on the molecular structure, and on the experimental resolution [3]. In the present work it was found that for $x > 1.0$ Å^{-1} no more oscillations were detected when considering an experimental resolution of about 0.1Å^{-1}.

Due to the complex dependence of the interference process on temperature and experimental setup, and due to the impossibility of knowing most of the molecular structure with the necessary accuracy, it is impossible to predict the exact limits for which the free model applies. Since within 10% no oscillation was detected for $x > 1.0$ Å^{-1}, it is possible to take 2.0 Å^{-1} as the limit. For more accuracy, a careful systematic measurement should be done.

ACKNOWLEDGMENTS

We would like to express our thanks to Dr. Wolfgang Jauch for providing access to the HMI spectrometer facilities and to Andreas Palmer for his kind helpfulness. We would also like to thank Dr. C. Cusatis and Dr. I. Mazzaro for providing helpful discussions. We are also grateful to Dr. L. Kissel for performing the theoretical calculations of Rayleigh cross sections, as well as for the careful revision of this paper. We are also indebted to the Deutscher Akademischer Austausch-Dienst (DAAD) for supporting the travel to Germany and to the Brazilian agencies CNPq, FAPERJ and FINEP for supporting the Brazilian part of the work.

[1] O. D. Gonçalves, I. Mazzaro, and C. Cusatis, IRPS News **4**, 9 (1990).

[2] J. Eichler, O. D. Gonçalves, and S. de Barros, Phys. Rev. A **37**, 3702 (1988).

[3] O. D. Gonçalves, C. Cusatis, and I. Mazzaro, Phys. Rev. A **48**, 4405 (1993).

[4] D. Schaupp *et al.*, J. Phys. Chem. Ref. Data **12**, 467 (1983).

[5] J. H. Hubbel *et al.*, J. Phys. Chem. Ref. Data **4**, 471 (1975).
[6] G. E. Brown, R. E. Peierls, and J. B. Woodward, Proc. R. Soc. London Ser. A **227**, 51 (1955).
[7] L. Kissel and R. H. Pratt, Phys. Rep. **140**, 75 (1986).
[8] P. P. Kanne, L. D. Kissel, R. H. Pratt, and S. C. Roy, Phys. Rep. **140**, 75 (1986).
[9] O. D. Gonçalves, J. Eichler, and S. de Barros, Nucl. Instrum. Methods A **280**, 375 (1989).
[10] L. V. Azároff, *Elements of X-Ray Crystallography* (McGraw-Hill, New York, 1968).
[11] J. R. Schneider, J. Cryst. Growth **65**, 660 (1983).
[12] L. Kissel (private communication).
[13] R. Kaplow, S. L. S. Strong, and B. L. Averbach, Phys. Rev. A **138**, 1336 (1965).